



**Supplementary Information for**

**Human hand as a powerless and multiplexed infrared light source for  
information decryption and complex signal generation**

Shun An, Wen Shang\*, Modi Jiang, Yini Luo, Benwei Fu, Chengyi Song, Peng Tao, Tao  
Deng\*

School of Materials Science and Engineering, Shanghai Jiao Tong University, 800  
Dongchuan Road, Shanghai, 200240, China

\*Wen Shang, Tao Deng

**Email:** [shangwen@sjtu.edu.cn](mailto:shangwen@sjtu.edu.cn), [dengtao@sjtu.edu.cn](mailto:dengtao@sjtu.edu.cn)

**This PDF file includes:**

Supplementary Text (Section 1-Section 11)

Figures S1 to S26

Table S1

Legend for Movie S1

SI References

**Other supplementary materials for this manuscript include the following:**

Movie S1

## Supplementary Text

### Section 1. Calculation of thermal radiation intensity of human hand and background

The thermal radiation intensity ( $M_\lambda$ ) at a specific wavelength ( $\lambda$ ) and temperature ( $T$ ) of a blackbody was calculated using Planck distribution function: (1)

$$M_\lambda(T)d\lambda = \frac{2\pi hc^2}{\lambda^5} \cdot \frac{1}{e^{hc/\lambda kT} - 1} d\lambda \quad (1)$$

where  $h = 6.626 \times 10^{-34}$  J s is Planck's constant,  $c = 2.998 \times 10^8$  m s<sup>-1</sup> is the speed of light in vacuum, and  $k = 1.38 \times 10^{-23}$  J K<sup>-1</sup> is the Boltzmann constant. For an object with the emissivity of  $\varepsilon(\lambda, T)$ , its thermal radiation intensity can be calculated by multiplying the emissivity with the  $M_\lambda(T)$  of the blackbody. The emissivity of human hand is ~0.98 (2) and the temperature of human hand is 310 K. The emissivity of background is 1 and the temperature of background is 298 K.

### Section 2. COMSOL simulation

The numerical simulation result shown in Fig. 1C was generated using COMSOL MULTIPHYSICS software. In the simulation, surface-to-surface radiation was used as the physics field. The temperature of the hand was set as 310 K and the emissivity was set as 0.98. In the simulation, a blackbody ( $\varepsilon = 1$ ) was set as the acceptor to receive the radiation from the hand. The temperature of the acceptor was set as 0 K, which means all the irradiance received by the acceptor was from the hand.

### Section 3. Mechanism of hand-based IR reflection for information decryption

In the IR imaging process, both the IR emission and IR reflection are collected by the IR detector as IR radiance. The IR radiance  $L$  collected from the sample can be calculated using Equation 2: (1)

$$L = \int_{\lambda_1}^{\lambda_2} \varepsilon_1 \cdot L_{\lambda}(T_1) d\lambda + \int_{\lambda_1}^{\lambda_2} R_1 \cdot L_{\lambda}(T_2) d\lambda \quad (2)$$

where  $\varepsilon_1$  is the emissivity of the sample,  $T_1$  is the temperature of the sample,  $R_1$  is the reflectivity of the sample,  $T_2$  is the temperature of background,  $\lambda_1 = 7.5 \mu\text{m}$  and  $\lambda_2 = 14 \mu\text{m}$ .  $L_{\lambda}(T)$  is the radiance of blackbody at the temperature of  $T$  and  $L_{\lambda}(T) = \frac{M_{\lambda}(T)}{\pi}$ . Here

we assumed that the background is a blackbody. Equation 2 includes the contribution from both the emission of the sample and also the reflected IR radiation from the background.

According to Kirchhoff's law, the amount of radiation absorbed by any object is equal to the amount of radiation that is emitted by this object: (1)

$$\varepsilon = \alpha \quad (3)$$

where  $\alpha$  is the absorptivity of the material.

The absorptivity of the material is related to both the transmissivity ( $t$ ) and reflectivity ( $R$ ):

$$\alpha + R + t = 1 \quad (4)$$

For the sample with the transmissivity ( $t$ ) of 0, the absorptivity and the emissivity can be calculated by Equation 5:

$$\varepsilon = \alpha = 1 - R \quad (5)$$

Combining equation (2) and (5) we obtain Equation 6:

$$L = \int_{\lambda_1}^{\lambda_2} L_{\lambda}(T_1) d\lambda + \int_{\lambda_1}^{\lambda_2} R_1 \cdot (L_{\lambda}(T_2) - L_{\lambda}(T_1)) d\lambda \quad (6)$$

For the sample that is composed of different regions with different reflectivity, if the temperature of background equals to the temperature of the sample ( $T_1=T_2$ ), the reflectivity ( $R_I$ ) of different regions has no effect on the radiance  $L$  (Equation 6). In the case when no hand is used in the IR decryption, the temperature of background equals to the temperature of the sample ( $T_1=T_2$ ) and thus different regions of the sample cannot be distinguished through IR decryption process even though their reflectivity is different. In the case when a hand is used as the background IR light source, the temperature of background ( $T_2$ ) is higher than that of the sample ( $T_1$ ), the IR radiance will be determined by the reflectivity ( $R_I$ ) of the sample with different regions. The IR detector will capture more IR radiance from the region with high reflectivity than the region with low reflectivity, which leads to the differentiation of IR radiances and enables the decryption process. Equation (6) also shows that what IR detector captures really represents the intensity distribution of IR radiance rather than the real temperature. We thus used the relative IR radiance to show the differences in IR radiance in the images captured by the IR detector. The relative IR radiance is defined as the ratio of the change of temperature reading in the IR detector to the maximum temperature difference, which is the difference between the hand temperature and the ambient temperature.

#### **Section 4. Experimental setup**

For the demonstration of using hand as an IR light source for reflection-based information encryption/decryption, the sample was placed on a horizontal working table (Fig. S2). The IR detector was fixed on a tripod and was 30 cm away from the sample. In

the experiment the IR detector was set at  $\sim 10^\circ$  from the axis perpendicular to the center of the sample. The hand or the LED light source was  $\sim 30$  cm away from the sample.

For the demonstration of using hand as a multiplexed IR light source for signal generation, the sample was placed on a horizontal working table (Fig. S9). The IR detector was fixed on a tripod and was 30 cm away from the sample. In the experiment the IR detector was set at  $\sim 10^\circ$  from the axis perpendicular to the center of the sample. The fingers of the hand were 10~15 cm away from the sample.

For the fixed position of detector and the sample, only IR radiation from specific angle and position can be detected by the IR detector and the rest IR radiation from human body will not interfere with the IR imaging.

For the direct visualization of hand gesture using visible or IR light, the IR detector (FLIR T620) or visible camera (Iphone 7) was placed 1.5 m away from the hand (Fig. S16).

## **Section 5. Comparison of the visible decryption and IR decryption**

FLIR T620 was used in both visible and IR decryption processes with the emissivity set to 1 during the IR decryption process. The detector in the visible detection mode was adjusted to have the same imaging resolution ( $640 \times 480$  pixels) as in the IR decryption process. The detector was fixed on a tripod and was 30 cm away from samples. The LED light (OPT-FL3729, OPT Machine Vision Tech Co., Ltd.) used in the visible decryption had a similar average radiation power in the visible range (400 nm ~700 nm) as the radiation power of human hand in the LWIR range ( $7.5 \mu\text{m} \sim 14 \mu\text{m}$ ). To obtain the IR radiation intensity of hand from  $7.5 \mu\text{m}$  to  $14 \mu\text{m}$  (the detectable wavelength range by the

IR detector), we calculated the corresponding blackbody radiation using Planck distribution function:

$$M_{\lambda}(T)d\lambda = \frac{2\pi hc^2}{\lambda^5} \cdot \frac{1}{e^{hc/\lambda kT} - 1} d\lambda \quad (7)$$

Here,  $h = 6.626 \times 10^{-34}$  J s is Planck's constant,  $c = 2.998 \times 10^8$  m s<sup>-1</sup> is the speed of light in vacuum,  $k = 1.38 \times 10^{-23}$  J K<sup>-1</sup> is Boltzmann constant,  $\lambda$  is the wavelength of the radiation, and  $T$  is the absolute temperature of the blackbody given in Kelvin, which is about 310 K for human hand. The corresponding blackbody radiation intensity was calculated by integrating the function from 7.5  $\mu$ m to 14  $\mu$ m. The emissivity of human skin is about 0.98, so the IR radiation from the hand was calculated by multiplying the blackbody radiation with the emissivity of the hand. The calculated radiation intensity of human hand was  $\sim 212$  W/m<sup>2</sup>. To make sure the radiation power of the hand was the same as the power of the LED lights (1.2 W), the radiation area of the hand should be  $\sim 60$  cm<sup>2</sup>. The front surface area of an adult hand is normally larger than 150 cm<sup>2</sup>. In the comparison experiments, we placed an Al foil with an open window of 60 cm<sup>2</sup> in front of the hand to ensure that the IR radiation power from the hand was comparable with the power of the visible light from the LED light source. The hand was put at the same position as the LED light, which was 30 cm away from the sample.

## **Section 6. Calculation of root-mean-square contrast (RMS<sub>contrast</sub>) of images**

To compare quantitatively the image contrasts recorded under different decryption approaches, all the images were converted into grayscale images first and then we calculated RMS<sub>contrast</sub> (Equation 8) (3) for all the grayscale images:

$$RMS_{contrast} = \sqrt{\frac{1}{MN} \sum_{i=0}^{N-1} \sum_{j=0}^{M-1} (I_{ij} - \bar{I})^2} \quad (8)$$

where intensity  $I_{ij}$  is the ( $i$ -th,  $j$ -th) element of the two-dimensional image with the size of  $M \times N$ .  $\bar{I}$  is the average intensity of all pixel values in the image. The image is assumed to have its pixel intensities normalized in the range [0, 1] so the  $RMS_{contrast}$  range is [0, 0.5](3).

For the demonstration purpose, in this work we also used a cell phone (iPhone 5C, Apple Inc., US) to scan images of the same QR code with different  $RMS_{contrast}$  (Fig. S3). If the information “SJTU” was scanned out, the corresponding image was decodable. The decodable  $RMS_{contrast}$  threshold value of  $\sim 0.042$  was obtained for the condition used in this study.

## Section 7. FDTD simulation of the grating diffraction

Grating diffractions were numerically simulated by the finite-difference time-domain (FDTD) method. The parameters of gratings were set based on the SEM images of gratings (Fig. 4B and Fig. S11). The boundary condition was set based on the assumptions that the light was absorbed (perfectly matched layer, PML) in the vertical direction and the gratings were periodic (periodic boundary condition, PBC) in the horizontal direction. The optical parameters of gratings were chosen as Al-CRC in database. A plane wave was used as the light source and the mesh size was  $0.1 \mu\text{m} \times 0.1 \mu\text{m}$ . The wavelength range was set as  $7.5 \mu\text{m}$  to  $14.0 \mu\text{m}$ . The simulated  $\theta_{in}$  ranges were marked in the 3D map (Fig. S12).



## Section 8. Image subtraction

The size of all the images was set as  $182 \times 128$  pixels and these images were converted into grayscale images by Matlab (MATLAB R2018a; MathWorks). For two different images, we calculated the absolute value of the grayscale difference pixel-by-pixel and the grayscale difference was converted into the subtracted image.

## Section 9. Calculation of Euclidean distance

Euclidean distance is commonly used to define the distance between two points in the  $m$ -dimensional space. For a gesture image, it can be viewed as a matrix ( $m \times n$ ) of the grayscale of the pixel. The Euclidean distance between image A and image B can thus be calculated by Equation 9: (4)

$$d = \sqrt{\sum_{i=1}^m \sum_{j=1}^n (x_{ij} - y_{ij})^2} \quad (9)$$

where  $x_{ij}$  and  $y_{ij}$  are the grayscale of pixel ( $i, j$ ) for image A and image B respectively.

## Section 10. Calculation of the two-dimensional (2D) information entropy

The 2D information entropy is used to characterize the amount of image data and it is defined by both the grayscale distribution and the spatial grayscale distribution of the image. At each pixel, the average grayscale value of the neighborhood can be calculated. The pixel grayscale and the average grayscale of the neighborhood form a pair. The probability of each pair is  $p_{ij}$ , so the 2D entropy can be calculated by Equation 10: (5)

$$E = -\sum_{i=0}^{255} \sum_{j=0}^{255} p_{ij} \log_2 p_{ij} \quad (10)$$

### **Section 11. Recognition of IA-HG (TFA)**

We used template matching to recognize IR patterns. Firstly, IR diffraction patterns were taken by the IR detector and were input into the graphical user interface (GUI) written using Matlab (MATLAB R2018a; MathWorks) in real time. Then IR images were cut to a specific size ( $182 \times 128$  pixels). For one image, we calculated the Euclidean distances of this image with preset 26 templates respectively (Fig. 5B) and the image was recognized as the template that had the shortest Euclidean distance with this image.

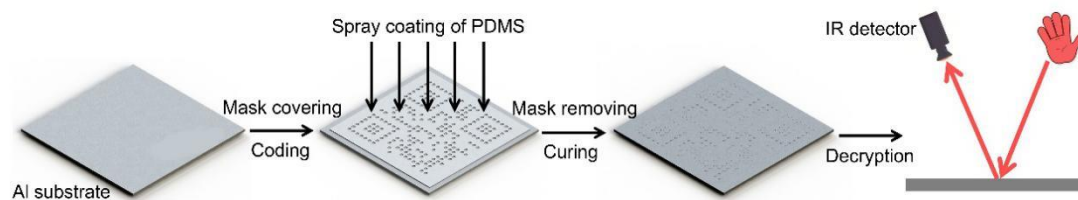


**Fig. S1. Schematic illustration of experimental process.**

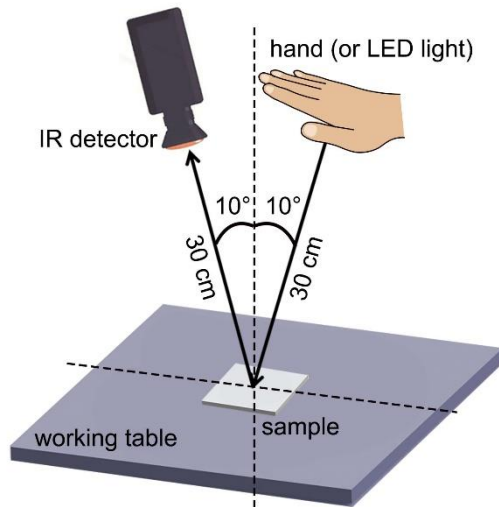


**Fig. S2. Experimental setup of using the whole hand as IR light source for the reflection-based information decryption.**

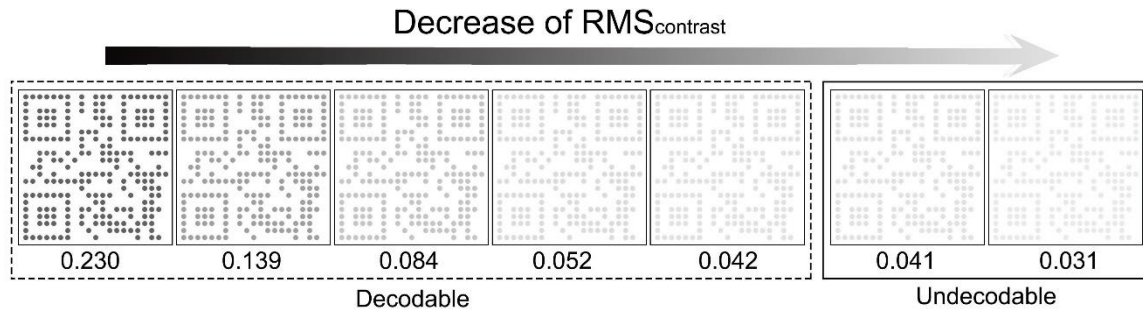


**Fig. S3. Coding patterns with different  $\text{RMS}_{\text{contrast}}$  (numbers represent the  $\text{RMS}_{\text{contrast}}$ ).**

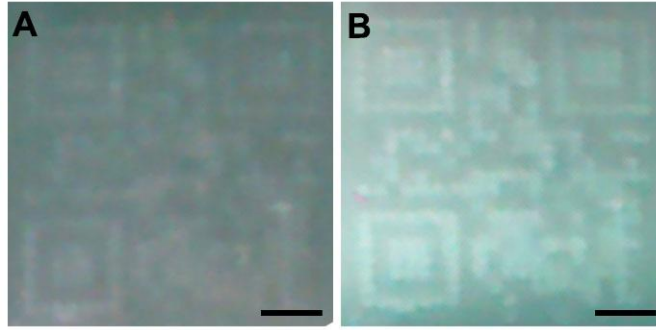


**Fig. S4. Visible images during the decryption process.** (A) Visible image of the coding pattern under the ambient light. (B) Visible image of the coding pattern with the LED light as the visible light source (scale bar: 5 mm).

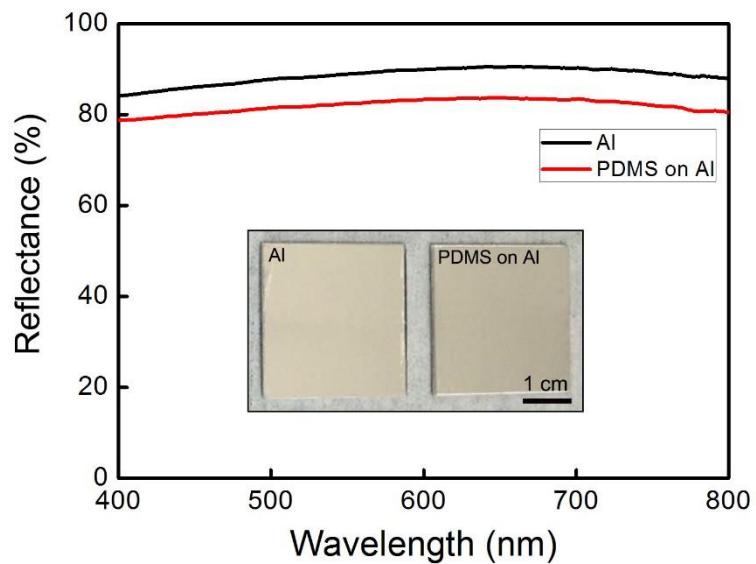


**Fig. S5. Reflectance spectra of Al sheet (~1 mm in thickness) and PDMS film (~3.0  $\mu\text{m}$  in thickness) on the Al substrate at visible range.**

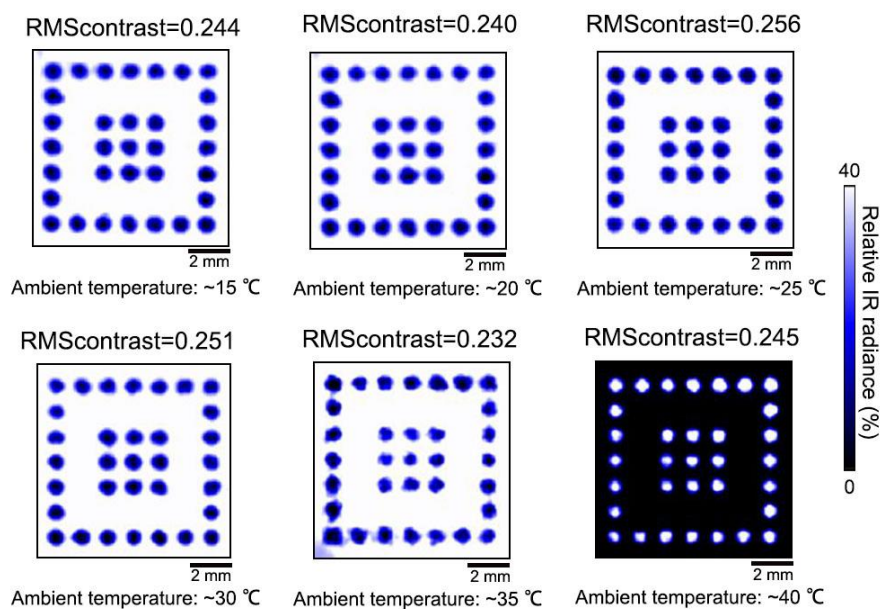


**Fig. S6. The IR images of coding pattern under different ambient temperature.**

When the ambient temperature is lower than the hand temperature, the patterned areas with PDMS show less IR radiance received by the IR detector, while the non-patterned areas with Al show higher IR radiance received by the IR detector. When the ambient temperature is higher than the hand temperature, the contrast is reversed, as shown in the image with ambient temperature at 40 °C.



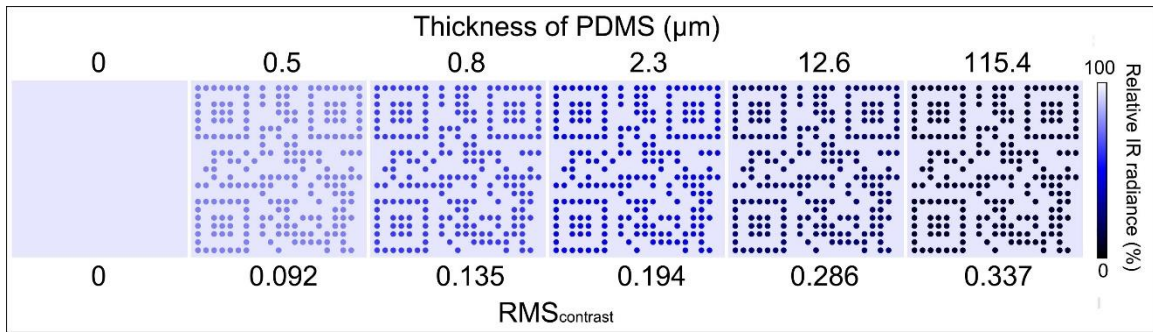


**Fig. S7. IR images of the same QR pattern made with different thickness of PDMS on Al substrates.** The relative IR radiance of PDMS with different thickness corresponds with a specific color in the color bar. We used these corresponding colors to generate these IR images. The corresponding  $\text{RMS}_{\text{contrast}}$  values were calculated for all the images.

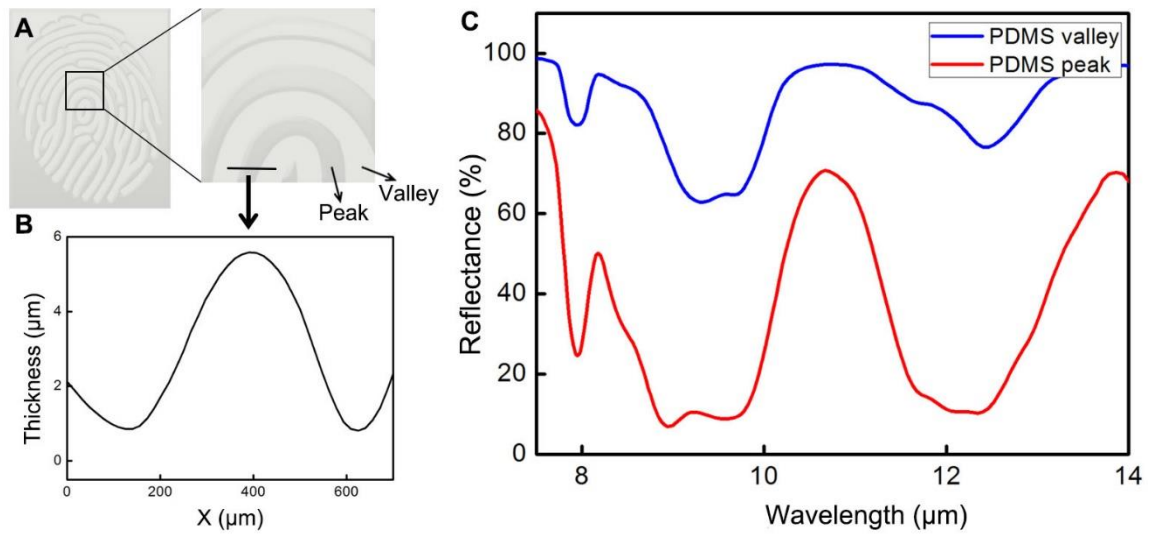


**Fig. S8. Fingerprint generated on PDMS.** (A) Schematic of the fingerprint. (B) The thickness of PDMS was measured across a peak area in the fingerprint in (A). (C) Reflectance spectra of PDMS at valley and peak areas.

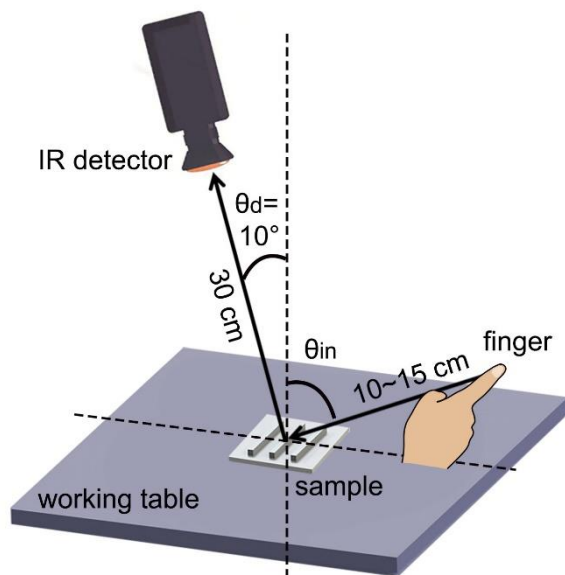


**Fig. S9. Experimental setup of using the hand as a multiplexed IR light source for the selective interaction with gratings.**  $\theta_{in}$  is the incident angle and  $\theta_d$  is the diffraction angle.

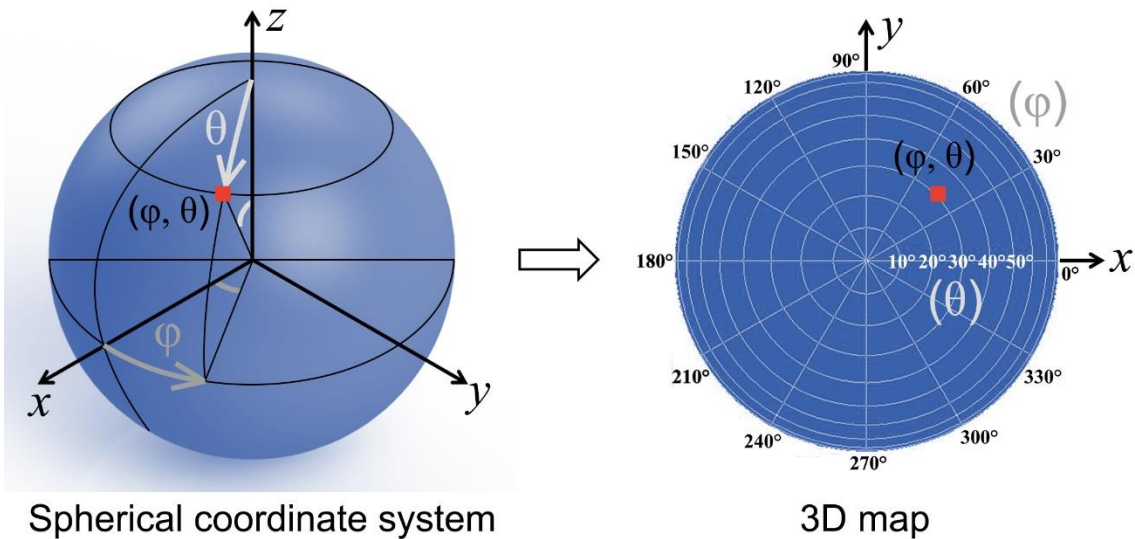


**Fig. S10. The relationship between the spherical coordinate system and the 3D map.**

The red dot  $(\varphi, \theta)$  in the spherical coordinate system corresponds to the red dot  $(\varphi, \theta)$  in the 3D map. The rings in the 3D map are not equally distanced. For the spherical coordinate system, the rings are equally distanced. When these rings are projected to a 2D plane, the rings are not equally distanced. The distance of adjacent two rings is decreased with the increase of the polar angle  $(\theta)$ . In the spherical coordinate system, the center of the sphere is set as the position of the sample (gratings). The  $xy$  plane is set as the horizontal plane that supports the sample. The  $z$  axis represents the direction perpendicular to the horizontal plane.

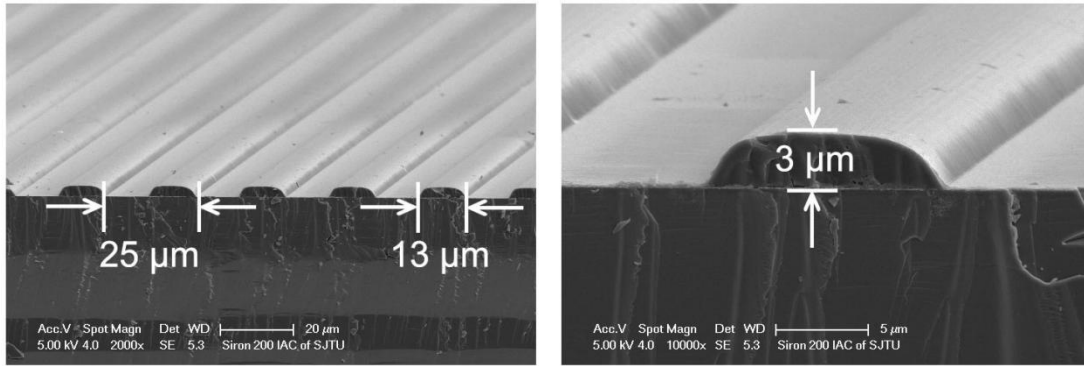


**Fig. S11. Cross-section SEM images of one of the gratings.**

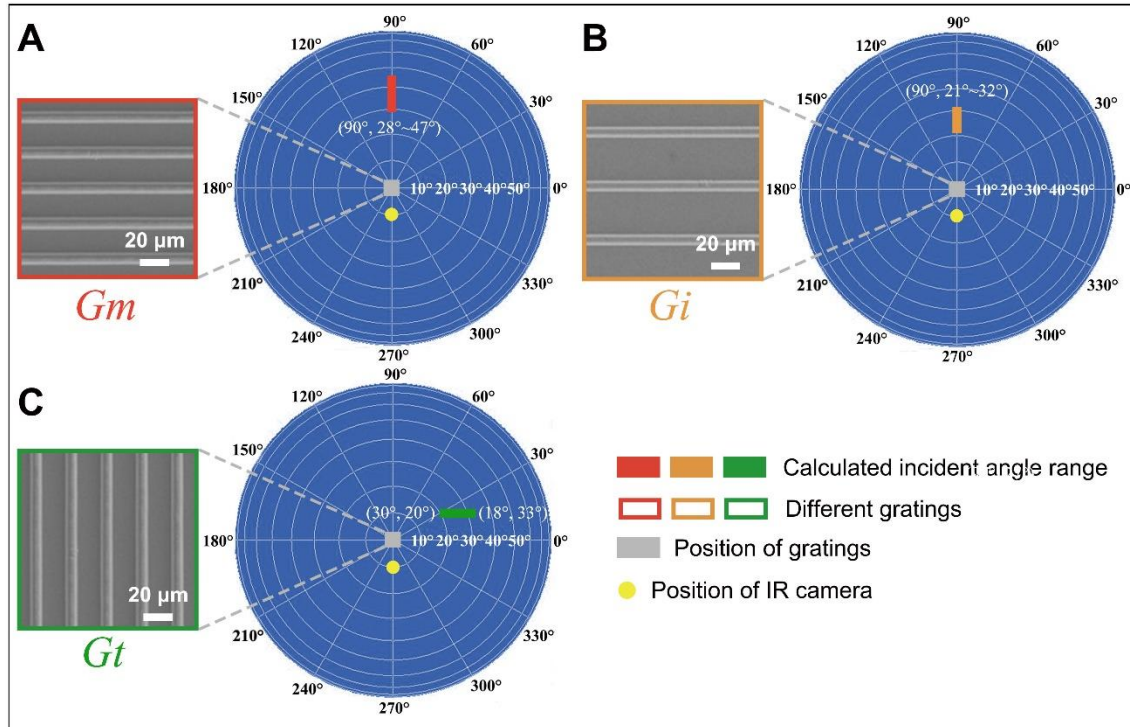


**Fig. S12. Effect of periods and orientations of gratings on diffraction.** (A-C) For specific  $\theta_d$  ( $\varphi = 270^\circ$ ;  $\theta = 10^\circ$ ) at  $-1^{\text{st}}$  diffraction, the incident angle ranges for gratings with different periods and orientations are marked in the 3D map.

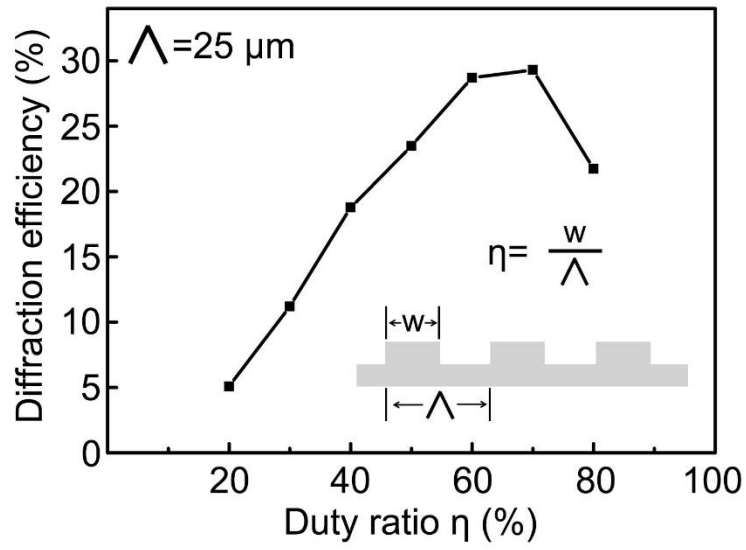
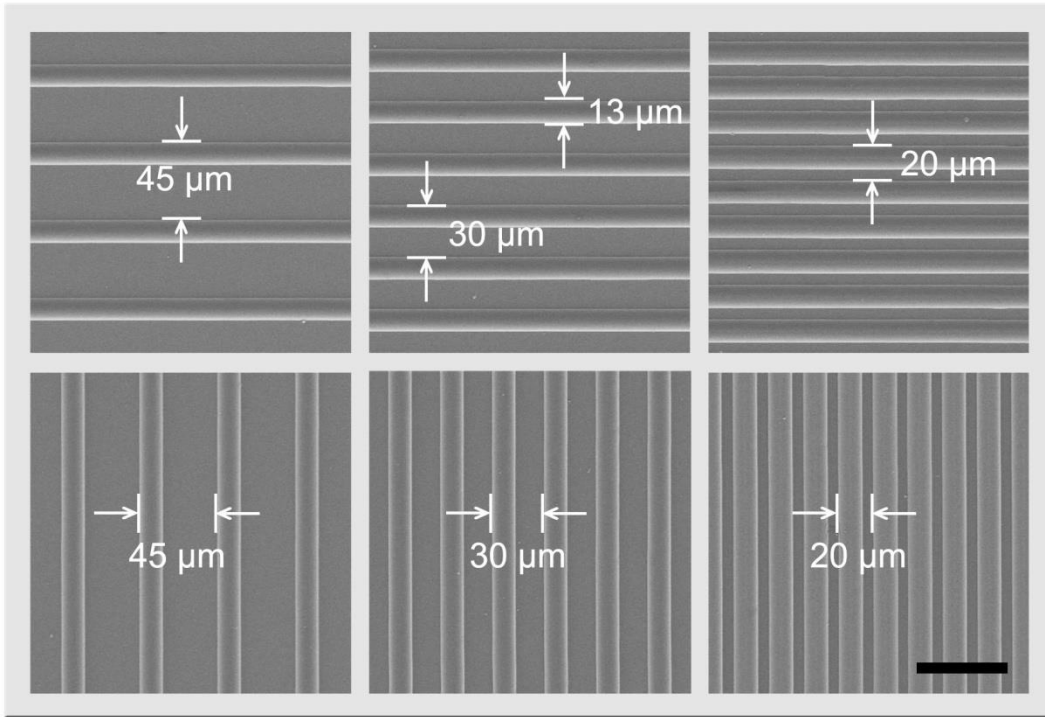


Fig. S13. FDTD simulation of the effect of duty ratio on diffraction efficiency.



**Fig. S14. SEM images of the designed patterns for sign language recognition (scale bar: 50 μm).**



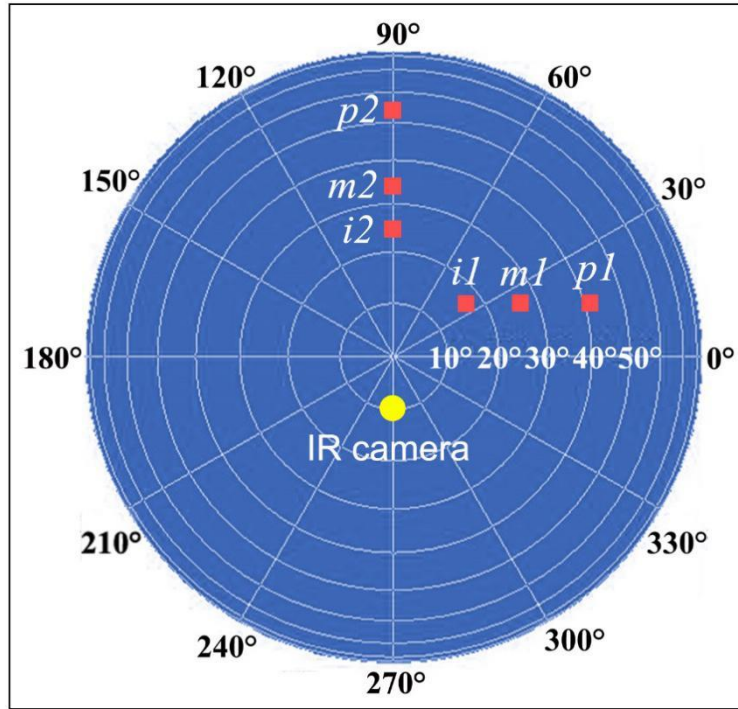
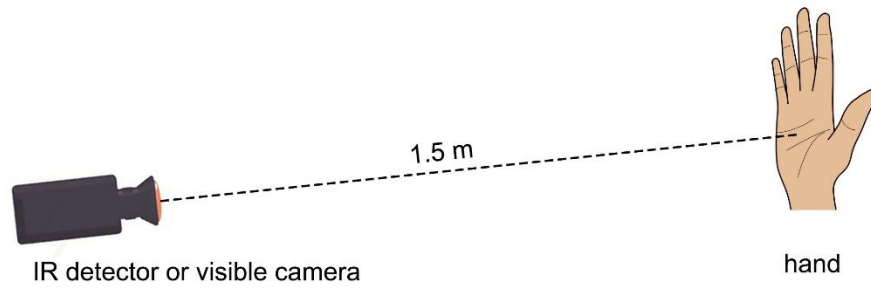
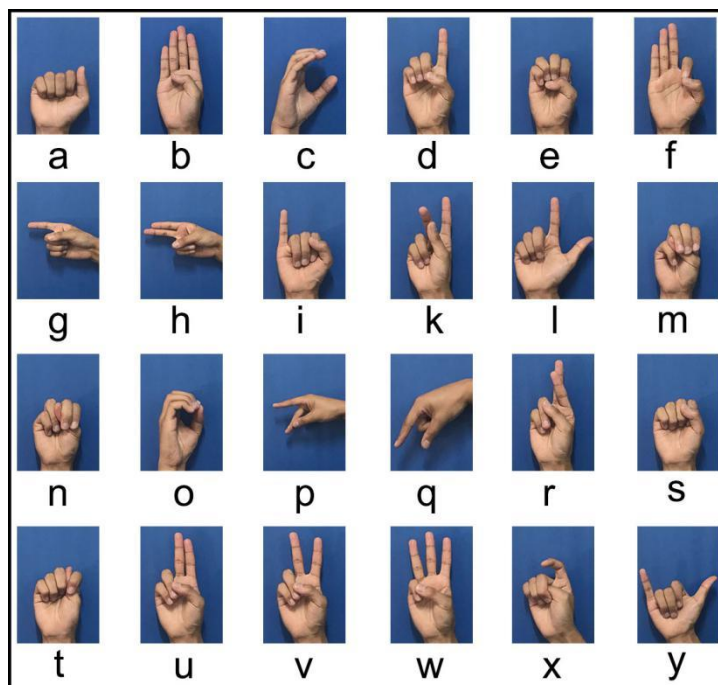


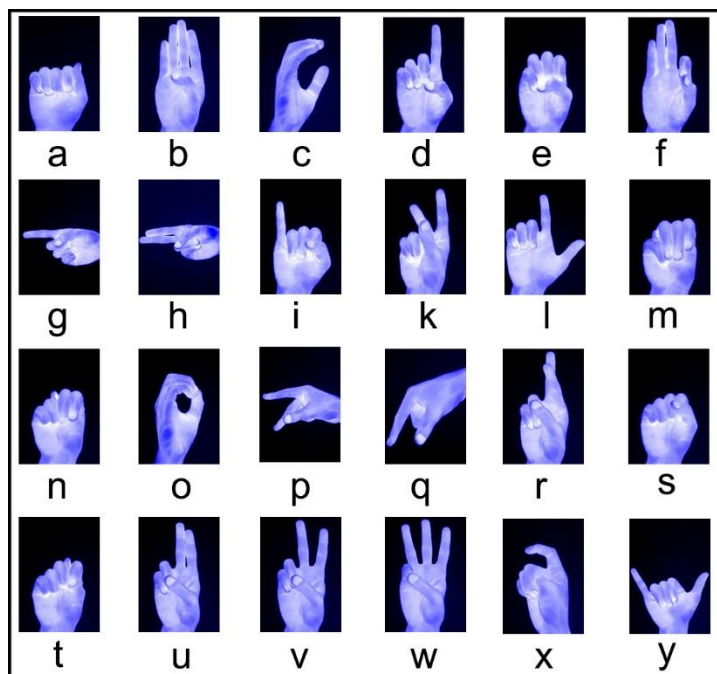
Fig. S15. 3D map of the positions of different fingers.



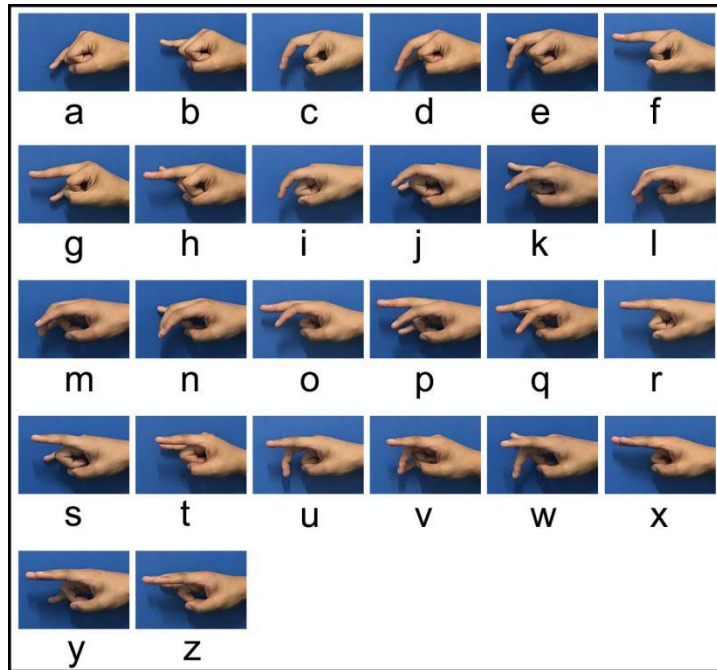
**Fig. S16. Experimental setup of the direct visualization of hand gesture using visible or IR light.**



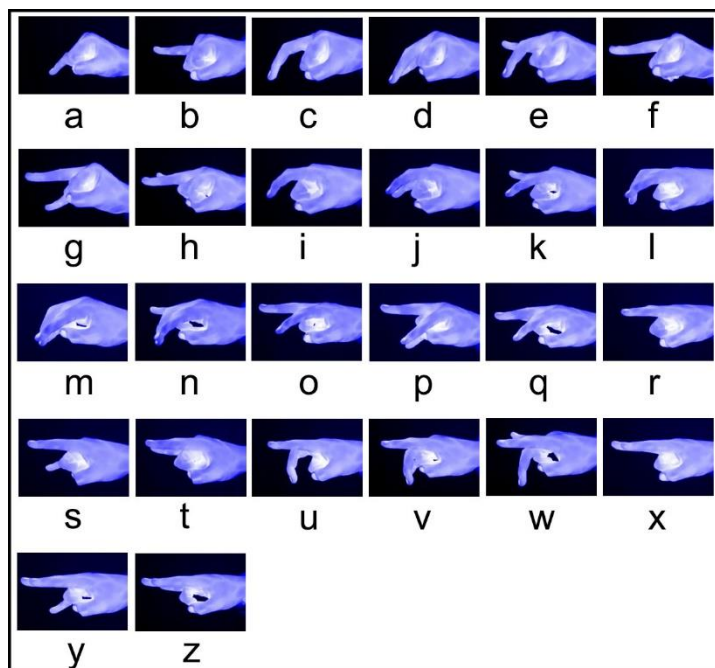
**Fig. S17. Visible images of AMA.**



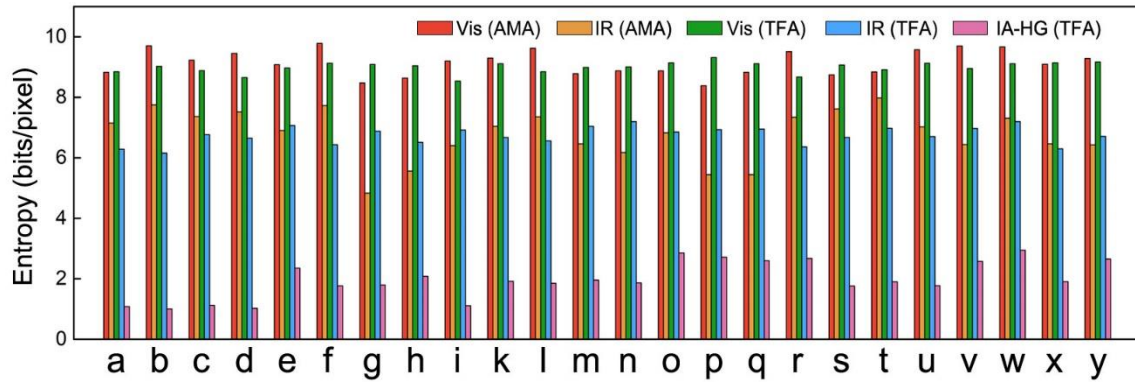
**Fig. S18. IR images of AMA.**



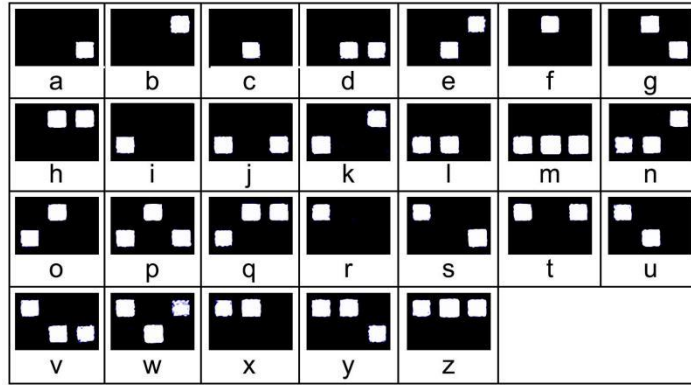
**Fig. S19. Visible images of TFA.**



**Fig. S20. IR images of TFA.**



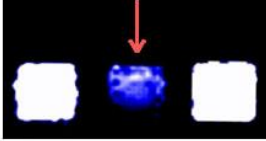


**Fig. S21. Entropy of alphabetic letters in different recognition systems.**



**Fig. S22. Sign language recognition in the dark using IA-HG (TFA).**



|                    |  |   |   |
|--------------------|--|---|---|
| image              | <p style="text-align: center; color: orange;">complete information</p>  | <p style="text-align: center; color: orange;">incomplete information</p>  | <p style="text-align: center; color: orange;">distracting information</p>  |
| recognition result | <p style="text-align: center;">“j” ✓</p>   | <p style="text-align: center;">“j” ✓</p>  | <p style="text-align: center;">“j” ✓</p>  |

**Fig. S23. Recognition ability with incomplete information or distracting information.**

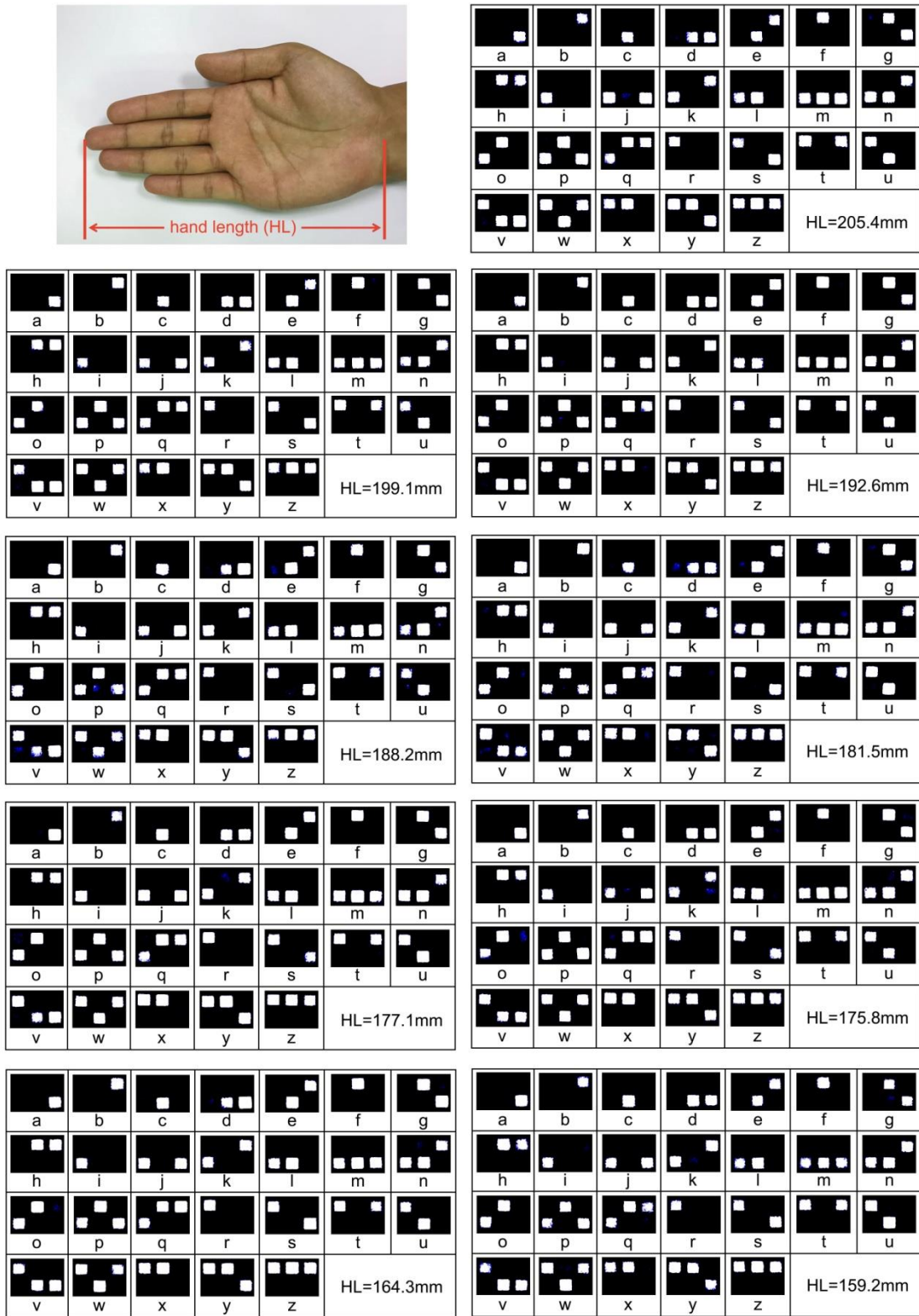
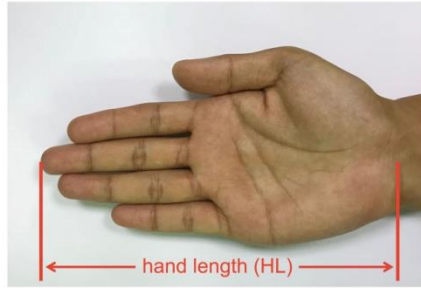
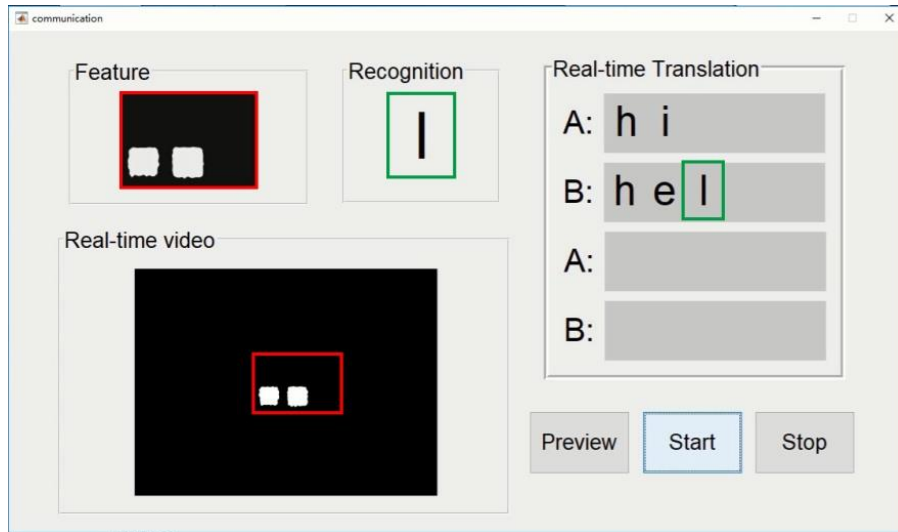
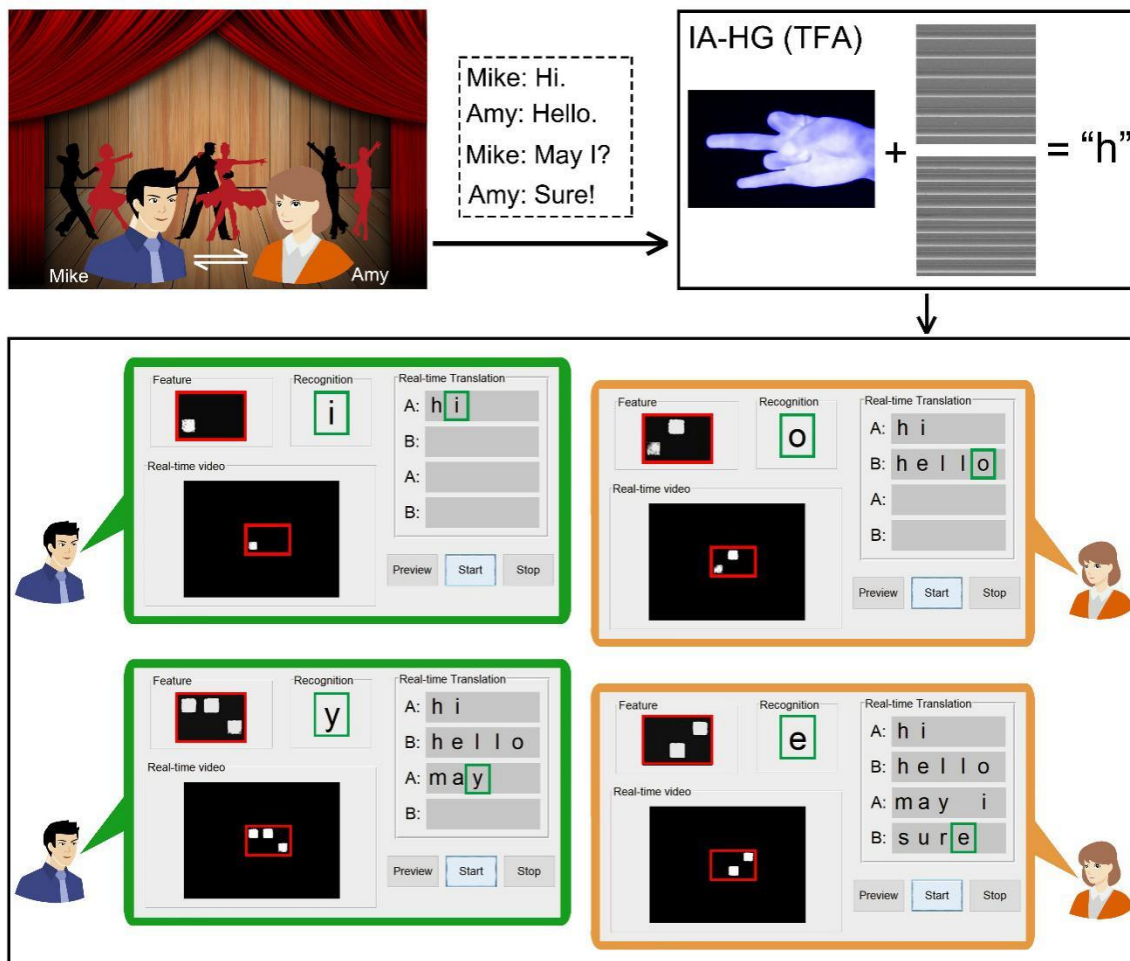


Fig. S24. Effect of the size of hand (hand length, HL) on sign language recognition.



**Fig. S25. GUI designed for real-time sign language recognition.**



**Fig. S26. Proof-of-concept demonstration of IA-HG (TFA) for real-time sign language recognition.** A GUI was used to collect IR diffraction patterns generated by gestures of two experimenters in real time and these IR images were recognized by the template matching method to simulate the scenario of an invitation for dancing.

**Table S1. The number of states for each finger in AMA and TFA.**

|                                | Thumb | Index finger | Middle finger | Ring finger | Pinkie | Total |
|--------------------------------|-------|--------------|---------------|-------------|--------|-------|
| American manual alphabet (AMA) | 5     | 8            | 9             | 7           | 5      | 34    |
| Three finger alphabet (TFA)    | 0     | 3            | 3             | 0           | 3      | 9     |

**Movie S1. Decryption of coding pattern without and with hand as IR light source.**

## SI References

1. V. Michael, K.-P. Mollmann, *Fundamentals of Infrared Thermal Imaging* (John Wiley & Sons, 2017).
2. V. Bernard, E. Staffa, V. Mornstein, A. Bourek, Infrared camera assessment of skin surface temperature-effect of emissivity. *Phys. Medica* **29**, 583-591 (2013).
3. E. Peli, Contrast in complex images. *J. Opt. Soc. Am. A* **7**, 2032-2040 (1990).
4. Y. Liu, L. Zhang, S. Zhang, A hand gesture recognition method based on multi-feature fusion and template matching. *Procedia Eng.* **29**, 1678-1684 (2012).
5. A. S. Abutaleb, Automatic thresholding of gray-level pictures using two-dimensional entropy. *Comput. Vis. Graph. Image Process.* **47**, 22-32 (1989).